International Journal of Thermal Sciences 48 (2009) 1923–1931

Contents lists available at ScienceDirect

International Journal of Thermal Sciences

journal homepage: www.elsevier.com/locate/ijts

Development of a finite element based heat transfer model for conduction mode laser spot welding process using an adaptive volumetric heat source

S. Bag [a,*], A. Trivedi [b], A. De [a]

[a] Mechanical Engineering Department, IIT Bombay, Powai, Mumbai, Maharashtra 400076, India
[b] Department of Production Engineering, B V M Engineering College, Vidyanagar, Gujrat 388120, India

ARTICLE INFO

Article history:
Received 12 April 2008
Received in revised form
13 December 2008
Accepted 17 February 2009
Available online 21 March 2009

Keywords:
Transient heat transfer
Laser spot welding
Finite element method
Adaptive volumetric heat source

ABSTRACT

Numerically computed results of weld pool dimensions in conduction mode laser welding are sensitive to the estimated value of the actual beam energy absorbed by the substrate. In a conduction based heat transfer analysis, the incorporation of the laser beam induced energy as a surface only heat flux fails to realize enhanced heat transfer in weld pool as molten material attains higher temperature and convective transport of heat becomes predominant. An alternate is to include fluid flow analysis considering phenomenological laws of conservation of mass and momentum that greatly increases the complexity in modeling. Uncertainty of material properties such as effective thermal conductivity and viscosity in the weld pool also impedes such extensive fluid flow analysis. A simpler and tractable approach can be to consider a volumetric heat source within weld pool in a conduction based heat transfer analysis. Earlier efforts to accommodate volumetric heat source such as double-ellipsoidal form remained unpopular since the size of the final weld pool shapes is required to be known to begin with the calculation. The present work describes an improved approach where a volumetric heat source is defined adaptively as the size of the weld pool grows in size within the framework of a conduction based heat transfer analysis. The numerically computed results of weld pool dimensions following this approach have shown fair agreement with the corresponding measured values for laser spot weld samples.

1. Introduction

Laser spot welding process has gained significance in multifarious fabrication industries due to its capability of producing precise weld pool shape with small heat affected zone. Since laser spot welding involves rapid melting and solidification of the substrate material along with very high peak temperature, it is difficult to experimentally monitor the in-process weld thermal cycle [1,2]. Precise knowledge of the weld thermal cycle experienced by the substrate is requisite to estimate the final microstructure and mechanical properties of the weld joint and the surrounding heat affected zone. Mathematical modeling of the laser spot welding process is traditionally preferred as an effective tool for *a-priori* estimation of the weld thermal cycle and subsequent weld quality. However, the modeling efforts face acute challenge in several aspects especially in terms of representing the laser beam as a heat source, accounting for the loss of material due to vaporization from weld pool, implementing reliable value of absorption coefficient, considering temperature dependence of material properties for solid as well as liquid material, incorporating latent heat and so on. The initial attempts to simulate laser beam welding process [3–9] were primarily based on Rosenthal's pioneering work [3]. The analytical models could not consider temperature dependent material properties and distributed heat flux corresponding to the laser beam.

Considerable work has been reported in the recent past to numerically simulate the laser beam welding process using both finite difference and finite element methods [10–19]. Mazumder and Steen [10] reported a three-dimensional, numerical model based on finite difference method to analyze heat transfer process in laser beam welding considering Gaussian heat flux distribution and constant thermophysical properties. Beer–Lambert's law was used to account for the absorption of laser energy inside the substrate thickness. The study showed that the spot diameter of laser beam and the assumed value of the absorption coefficient could

* Corresponding author. Mechanical Engineering Department, IIT Bombay, Powai, PS-21, Tulsi Block, Mumbai, Maharashtra 400076, India. Tel.: +91 22 25767509; fax: +91 22 25726875.
E-mail address: t_swarup@iitb.ac.in (S. Bag).

1290-0729/$ – see front matter © 2009 Elsevier Masson SAS. All rights reserved.
doi:10.1016/j.ijthermalsci.2009.02.010

Nomenclature

a, b	instantaneous value of ellipsoidal axis
C_p	specific heat
d	power density distribution factor of laser beam
$\{f\}$	thermal load vector in finite element formulation
h	convective heat transfer coefficient
k	thermal conductivity
L	latent heat
N_i	elemental shape functions
N_H	non-dimensional heat index
P	power of laser beam
p_i	instantaneous value of weld penetration
q_s	surface heat flux
$\dot{Q}$	heat input per unit time per unit volume
r	radial axis in cylindrical coordinate system
r_{eff}	effective laser beam radius
t	temporal coordinate
T	temperature variable
T_0	ambient temperature
T_i	nodal temperature variable
T_L, T_S	liquidus and solidus temperature
w_i	instantaneous value of half weld width
z	axial direction in cylindrical coordinate system

Greek symbols

ε	emissivity
ρ	density
σ	Stefan–Boltzmann constant
Γ	elemental surface area
Ω	elemental volume
η_{gau}	absorption coefficient for surface heat flux
η_{vol}	absorption coefficient for volumetric heat source

significantly influence the computed weld dimensions. Zacharia et al. [11] included the analysis of convective heat transfer in a laser weld pool. The two-dimensional finite difference based numerical model showed the influence of the surface tension gradient on the convective heat transport and the computed weld pool dimensions [11]. Pitscheneder et al. [12] developed a conduction based finite difference model representing laser beam as a Gaussian surface heat flux and constant thermophysical properties. Enhanced heat transfer in weld pool due to heat convection was accounted for by artificially increasing the thermal conductivity by a factor of seven. He et al. [13] included both the conduction and the convective heat transfer in laser weld pool, and the influence of surface tension gradient while the material properties were considered to be independent of temperature. Based on extensive numerical calculations, it was reported that the temperature gradient and the rate of cooling in weld pool would be much larger in a laser weld pool in comparison to a gas tungsten arc weld pool.

In their conduction based heat transfer model Goldak et al. [14] initiated the concept of volumetric source in fusion arc welding and suggested its use for high penetration laser beam welding to account for the enhanced heat transfer. The volumetric heat source was conceptualized by defining a pseudo weld pool in the form of an ellipsoid, receiving heat energy due to a welding arc or laser beam from the beginning of the weld time. The intensity of energy in the pseudo weld pool was considered to reduce exponentially both in the axial and radial directions. Although the consideration of a volumetric heat source could improve the accuracy of the numerical prediction of weld pool sizes in high power welding, one specific problem remained with quantitatively defining the size of the pseudo weld pool (i.e. the volumetric heat source) *a-priori*. De et al. [15,16] had presented a finite element based numerical model to analyze laser spot welding process considering a volumetric heat source with conduction mode heat transfer only. The temperature dependence of material properties and influence of phase change were incorporated. Although the authors could calculate weld pool shapes, cooling rate and expected mechanical properties in weld, it was indicated clearly that extensive trial-and-errors were necessary to fix up the size of the volumetric heat source as *a-priori*. Frewin and Scott [17] reported a finite element based numerical model for pulsed laser welding considering heat conduction only. The authors had measured the laser beam profile experimentally and a similar heat intensity distribution was used in the numerical calculations. It was concluded that the input of the experimentally measured heat intensity distribution led to better predictions of the weld pool dimensions. Numerical models considering both conduction and convective modes of heat transfer in weld pool are proved to be more accurate in estimating specific shapes and dimensions of the weld pool. However, such models are inherently complex and require a number of input parameters such as effective thermal conductivity, and viscosity of weld pool material that are rarely available.

Numerical models considering only the conduction mode of heat transfer cannot account for the enhanced heat transfer in weld pool that occurs due to convective heat transport driven by Marangoni force. However, such models are simple and can provide fairly accurate estimation of weld pool provided the enhanced heat transfer within molten weld pool is accounted for. This has been the motivation of the present study. An improved approach is attempted to consider a volumetric heat source adaptively in a finite element based heat conduction model for laser spot welding. The volumetric heat source is considered to be dynamic in nature and is linked with the growing weld pool size so that no *a-priori* definition of a pseudo weld pool is necessary. The material properties are considered to be temperature dependent. The influence of phase change has been incorporated.

It is imperative to say that the conduction based models fail to realize the weld pool shape when the material contains surface active elements such as sulfur in steels. Such active elements change the magnitude and direction of surface tension force and hence the shape of weld pool geometry. To treat the same, a full fledged coupled heat transfer and fluid flow simulation is essential [12,13]. Thus, the conduction mode heat transfer model with adaptive volumetric heat source in the present effort is limited to the material containing no surface active elements or very little surface active elements. Moreover, in the present model, the free surface of solution geometry is assumed flat and there is no deformation of free surface.

2. Heat transfer simulation

The heat transfer in the substrate is conceived to be two-dimensional axisymmetric in nature considering the axial symmetry of the laser beam. Fig. 1 shows two-dimensional transverse section from a typical but joint configuration analyzed in the present work and the associated boundary conditions are also described in this figure. The governing heat conduction equation in cylindrical coordinate system can be specified as

$$\frac{1}{r}\frac{\partial}{\partial r}\left(kr\frac{\partial T}{\partial r}\right)+\frac{1}{r}\frac{\partial}{\partial z}\left(kr\frac{\partial T}{\partial z}\right)+\dot{Q}=\rho C_p\frac{\partial T}{\partial t} \tag{1}$$

where r and z refer to radial and axial directions; k, ρ, and C_p respectively refer to thermal conductivity, density, and specific heat of material; T and t refer to temperature and time variable

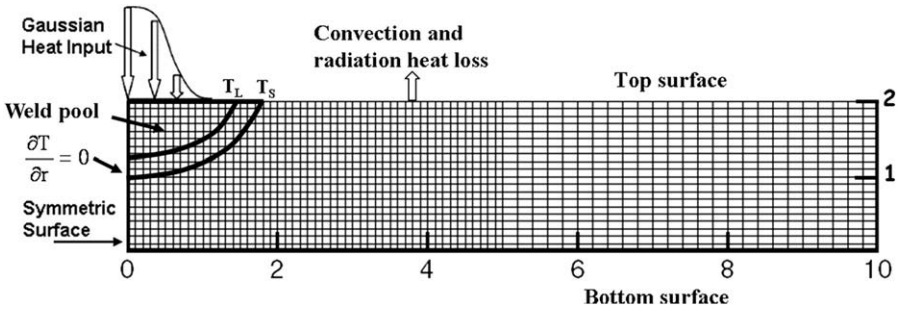

Fig. 1. Schematic plot of the finite element mesh of the solution domain along with boundary conditions.

respectively, and $\dot{Q}$ depicts internal heat generation per unit time and unit volume. The associated boundary condition (Fig. 1) can be stated as

$$k\frac{\partial T}{\partial n} - q_s + h(T - T_0) + \sigma\varepsilon\left(T^4 - T_0^4\right) = 0 \tag{2}$$

where k refers to thermal conductivity normal to surface; h and ε depict surface heat transfer coefficient and emissivity respectively; σ is Stefan–Boltzmann constant, and T_0 is the ambient temperature. The first, third and fourth terms in the left hand side of equation (2) respectively refer to conductive, convective and radiative heat loss from the surface of the substrate. The term q_s stands for the imposed heat flux onto the surface due to the laser beam. To avoid the non-linearity due to the term arising out of radiative heat loss, a lumped heat transfer coefficient is used combining the convective and radiative heat loss by considering h, as [20]

$$h = 2.4 \times 10^{-3}\varepsilon T^{1.61} \tag{3}$$

where h is in $\mathrm{W\,m^{-2}\,K^{-1}}$, T is in K and ε is the emissivity. The heat input into the substrate due to the application of laser beam is considered in terms of surface heat flux [through the term q_s in equation (2)] till the top surface of substrate is below solidus temperature as

$$q_s = \frac{P\eta_{gau}d}{\pi r_{eff}^2}\exp\left(-\frac{dr^2}{r_{eff}^2}\right) \tag{4}$$

where P refers to beam power, η_{gau} absorption coefficient, r_{eff} the effective radius of the laser beam and d is the distribution coefficient related to the pattern of the laser beam profile. As the substrate subsequently melts, the surface heat flux is replaced by a volumetric heat source expression for the portion of the molten substrate as

$$\dot{Q} = \frac{6\sqrt{3}P\eta_{vol}}{\pi\sqrt{\pi}a^2 b}\exp\left(-\frac{3r^2}{a^2} - \frac{3z^2}{b^2}\right)$$
$$\text{where } \begin{cases} a = r_{eff} & \text{for } a \le r_{eff} \\ a = w_i & \text{for } a > r_{eff} \\ b = p_i & \end{cases} \tag{5}$$

where $2w_i$ and p_i represent the instantaneous values of the computed width and penetration of the weld pool respectively obtained from the numerical calculations. η_{vol} is the absorption coefficient of volumetric heat. Here, the volumetric heat source follow the shape defined by an ellipsoid (eq. (5)) having axis a and b since, in general, the conduction mode weld pool profile follow more close to this shape [14–18]. Moreover, the volumetric efficiency, η_{vol} can accommodate the mismatch between the actual weld profile and assumed ellipsoidal profile in the calculation of volumetric heat. It is apparent from equation (5) that the values of a and b change accordingly as the weld pool grows in size. Furthermore, equation (5) does not need *a-priori* knowledge of the final weld pool shape that is otherwise required in similar expressions used earlier [14–16]. The heat input obtained from equation (5) is applied directly into the weld pool volume through the term $\dot{Q}$ in equation (1). Fig. 2 schematically shows the expected shape of the energy distribution within the volumetric heat source. Since one-half of the substrate is considered as the domain of analysis considering the symmetry of a stationary laser beam, a symmetric boundary condition is defined along z-axis as

$$\frac{\partial T}{\partial r} = 0 \tag{6}$$

As, the process is transient in nature, an initial condition is defined at time $t = 0$ as

$$T(r, z, 0) = T_0 \tag{7}$$

3. Finite element discretization

The elemental discretization of the solution domain is described in Fig. 1 that is characterized by a rectangular region of 10 mm (width) and 2 mm (thickness). Four node isoparametric elements are used for geometry discretization. Near to the laser beam, very small elements of size 0.1 mm × 0.1 mm (Fig. 1) are used while away from the beam (beyond a distance

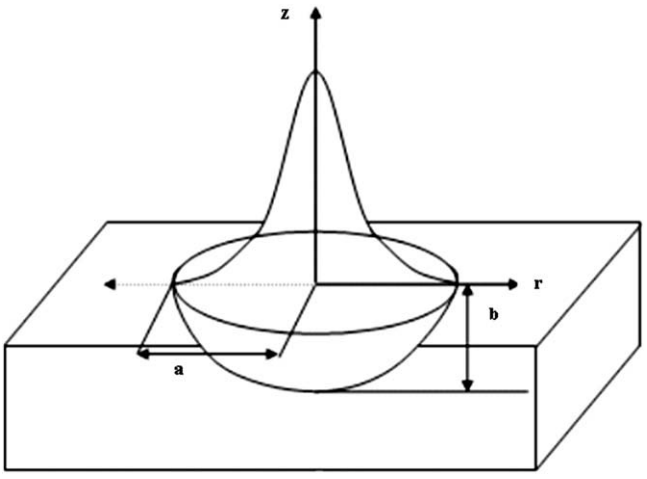

Fig. 2. Schematic plot of adaptive volumetric heat source and associated energy distribution.

of 5.0 mm in the width direction) larger elements as 0.2 mm × 0.1 mm are used to economize the total number of elements and nodes for the complete geometry. The governing equation (1) along with the boundary conditions equation (2) are discretized in spatial and time-coordinate systems following Galerkin's weighted residue technique in finite element method. Within each iso-parametric element, temperature variable $T(r, z)$ is expressed as

$$T = \sum_{i=1}^{4} [N_i]\{T_i\} \tag{8}$$

where N_i is the elemental shape functions and T_i is corresponding nodal temperature. The governing equation with associated boundary condition can be represent in matrix form for any specific element 'e' as

$$[H^e]\{T\} + [S^e]\left\{\frac{\partial T}{\partial t}\right\} + [\overline{H}^e]\{T\} + \left\{f_{\dot{Q}}^e\right\} + \left\{f_q^e\right\} + \{f_h^e\} = 0 \tag{9}$$

where the general term of the matrices can be given as

$$[H_{ij}^e] = \int_{\Omega^e} k\left(\frac{\partial N_i}{\partial r}\frac{\partial N_j}{\partial r} + \frac{\partial N_i}{\partial z}\frac{\partial N_j}{\partial z}\right)\mathrm{d}\Omega \tag{10}$$

$$[S_{ij}^e] = \int_{\Omega^e} \rho C N_i N_j \mathrm{d}\Omega; \quad \left[\overline{H}_{ij}^e\right] = \int_{\Gamma^e} hN_iN_j\mathrm{d}\Gamma \tag{11,12}$$

$$\left\{\left(f_q^e\right)_i\right\} = -\int_{\Gamma_1^e} N_i q_s \mathrm{d}\Gamma; \quad \{(f_h^e)_i\} = -\int_{\Gamma_2^e} N_i h T_0 \mathrm{d}\Gamma \tag{13,14}$$

$$\left\{\left(f_{\dot{Q}}^e\right)_i\right\} = -\int_{\Omega^e} N_i \dot{Q}\,\mathrm{d}\Omega \tag{15}$$

where $i, j = 1, 4$. Considering the contribution from all the elements within the domain as well as along the surface, the final algebraic equation can be written as [21]

$$[H]\{T\} + [S]\left\{\frac{\partial T}{\partial t}\right\} + [\overline{H}]\left\{T\right\} + \left\{f_{\dot{Q}}\right\} + \left\{f_q\right\} + \{f_h\} = 0 \tag{16}$$

Considering the similar dimension of the generated matrix, eq. (16) can be rewritten as

$$[\overline{\overline{H}}]\{T\} + [S]\left\{\frac{\partial T}{\partial t}\right\} + \left\{f\right\} = 0 \tag{17}$$

where,

$$[\overline{\overline{H}}] = [H] + [\overline{H}]; \quad \{f\} = \left\{f_{\dot{Q}}\right\} + \left\{f_q\right\} + \left\{f_h\right\} \tag{18,19}$$

Equation (17) is further discretized in time zone as

$$\{T\}_{n+1} = -\left[\frac{2}{3}[\overline{\overline{H}}] + \frac{1}{\Delta t}[S]\right]^{-1}\left\{\left[\frac{1}{3}[\overline{\overline{H}}] - \frac{1}{\Delta t}[S]\right]\{T\}_n + \{f\}\right\} \tag{20}$$

where t refers to time, Δt refers to time increment, $\{T\}_{n+1}$ and $\{T\}_n$ are nodal temperature vectors corresponding to $(n+1)$-th and n-th time steps respectively.

The latent heat of melting and solidification is included in this simulation through an increase or decrease in the specific heat of the material. The specific heat C_p is considered in the present model as

Table 1
Chemical composition (in wt%) of low-carbon steel sheets.

C	Si	Mn	Cr	Ni	V	Mo
0.07	0.10	0.92	0.04	0.03	<0.01	<0.01

$$\left.\begin{aligned} C_p &= C_1 && \text{for } T < T_S \\ C_p &= C_2 && \text{for } T > T_L \\ C_p &= C_m = \frac{L}{(T_L - T_S)} + \frac{(C_1 + C_2)}{2} && \text{for } T_S \le T \le T_L \end{aligned}\right\} \tag{21}$$

where L is latent heat, T_S and T_L are solidus and liquidus temperatures respectively. For an element of volume undergoing phase change the specific heat is obtained as a weighted average of the associated specific heats; viz. C_1 and C_m (for solid to mushy state or the reverse), C_m and C_2 (for mushy to liquid state or the reverse) or C_1, C_m and C_2 (for a jump from solid to liquid state or the reverse). The software program for the two-dimensional axisymmetric heat transfer analysis is developed using INTEL Fortran Compiler. The results of temperature field are viewed and plotted using Tecplot software.

4. Results and discussions

To validate the computed results from the numerical model and the general applicability of the adaptive volumetric heat source, several laser spot welding experiments are carried out considering a wide range of beam power, spot diameter and on-times. In addition, the numerical model is also validated with a set of experimentally measured laser spot welded dimensions reported in independent literature [22]. Table 1 presents the chemical composition of the low-carbon steel sheets which are used in reference [22]. The sheet materials used in the present experiments also confirm to similar chemical compositions. Table 2 depicts the welding process parameters corresponding to both the in-house experimental studies and the reported experimental results [22]. It is noteworthy that the overall combinations of laser power and spot radii, which are used to validate the numerical model, confirm to a wide range of power density from 0.8 to 2.8 kW/mm^2. Pulsed Nd:YAG laser beam is used for the in-house experimental studies while a diode laser has been used in reference [22]. Fig. 3 shows the temperature dependent material properties that are considered in the numerical calculations. The values of absorption coefficient (η_{gau}), volumetric efficiency (η_{vol}) and beam distribution coefficient (d) are considered to be 0.30, 0.35 and 3.0 to compute weld pool dimensions corresponding to all the experimental welding conditions.

Fig. 4(a)–(d) presents a comparison of the calculated and the corresponding measured weld pool shapes made at four different combinations of process parameters. In each of these figures, the picture on the left depicts the measured weld pool with a white or

Table 2
Combinations of welding process parameters corresponding to different sheet thicknesses.

Laser power (kW)	Effective radius (mm)	Power density (kW/mm^2)	Sheet thickness (mm)	Laser on-time (ms)
1.00	0.63	0.8	0.8	6, 8, 10, 12, 14, 16, 18, 20
1.60	0.63	1.3	1.0	6, 8, 10, 12, 14, 16, 18, 20
1.40[a]	0.5	1.8	2.0	150, 650,1150, 1650, 2150, 2650
2.23[a]	0.5	2.8	2.0	150, 165, 180, 195, 210, 225

[a] Taken from independent literature [22].

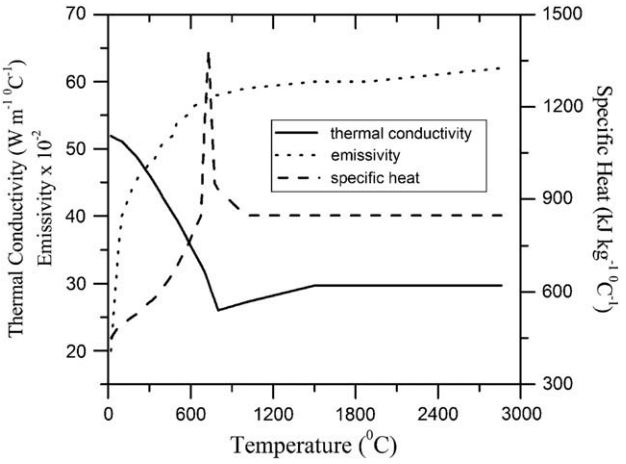

Fig. 3. Temperature dependent material properties [17].

black line denoting the boundary of the molten zone and the plot on the right depicts the computed weld pool in terms of the temperature isotherms. The zone encompassed by the isotherm A (liquidus temperature ≈ 1773 K) depicts the fusion zone and its intercepts on *z*- and *r*- axes indicate the penetration, *p* and the half-width, *w* respectively. The region encompassed in between the isotherms *A* (≈1773 K) and *C* (≈996 K) can be considered as the computed heat affected zone. It is noteworthy that the laser power and spot radius corresponding to Fig. 4(a) and (b) confirm to a power density of 1.3 kW/mm^2 while that of Fig. 4(c) and (d) confirm to 1.8 kW/mm^2. Fig. 4(a)–(d) indicates that the numerically computed weld pool shapes are in fair agreement with the corresponding experimentally measured weld pools for a range of power densities.

In general, the steep temperature gradient from the center to the periphery of the free surface of the weld pool sets negative surface tension gradient that tends to promote enhanced convective heat transport in the radial direction. Consequently, the size of the melt pool increases more in the radial direction in comparison to the axial direction [12]. In the present model, an enhanced value of thermal conductivity (five times of the same at liquidus temperature) is considered for the topmost layer of elements to simulate a similar phenomenon although finding a single value of enhancement factor in thermal conductivity corresponding to all the sets of process parameters considered in this work has been a tedious task. It can be mentioned that Pitscheneder et al. [12] considered an enhancement factor of seven and Hong et al. [19] used a factor of ten in thermal conductivity in their reported models. The present value of enhanced conductivity is thus comparable to the earlier studies [12,19].

It is clear from the measured weld profiles in Fig. 4(a) and (b) that the weld pool aspect ratio (i.e. *p*/2*w*) increases from 0.21 to 0.27 as the on-time is enhanced from 10 to 14 ms. Similarly, the weld pool aspect ratio is enhanced from 0.37 to 0.42 (nearly semi-circular weld) as the on-time is enhanced from 0.15 to 0.65 s at a laser power of 1.4 kW as observed in Fig. 4(c) and (d) respectively. The enhancement in the weld pool aspect ratio with the increase in on-time is resulted by the greater increase in the penetration in comparison to the weld width. At higher on-time, the substrate volume beneath the laser is exposed to the beam for a longer time that increases effective absorption of total beam energy. Subsequently, the peak temperature of the weld pool increases thereby enhancing also the downward axial heat transfer resulting in greater penetration. A small crater at the top of the measured weld pool in Fig. 4(d) also indicates loss of substrate material due to vaporization that might have been caused by the combined effect of high power density and high peak temperature. However, the loss of bulk material owing to vaporization is not incorporated in the present model for simplicity. The measured weld pool shapes in Fig. 4(a)–(c) indicate a typical conduction mode laser spot welding with small aspect ratio (i.e. *p*/2*w*) while the weld pool in Fig. 4(d) tends to indicate a keyhole mode laser spot weld with nearly semi-circular melt pool.

Fig. 5 shows a comparison of the experimental and the computed weld dimensions at varying laser on-times corresponding to four different power densities (Table 2). In each case, the measured weld pool aspect ratio (i.e. *p*/2*w*) is also plotted. It is observed that the computed weld pool dimensions are in well agreement with the corresponding measured results for laser power of 1.0 kW, 1.6 kW and 1.4 kW [Fig. 5(a)–(c)]. However, the

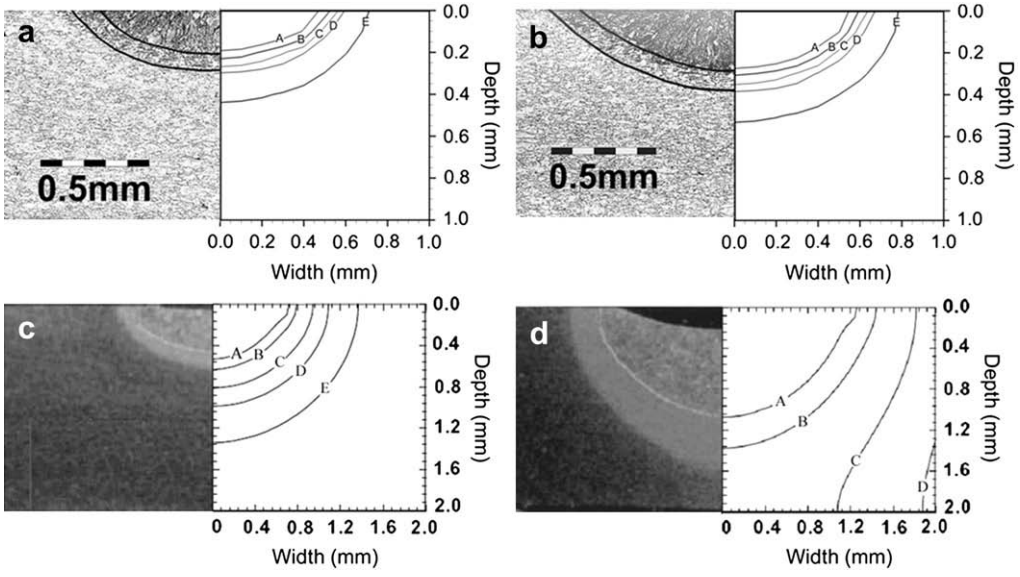

Fig. 4. Comparison of experimental (left) and computed (right) fusion zone for different combinations of beam power (*P*), spot radius (r_{eff}) and on-time (t_{on}). (a) P: 1.6 kW, r_{eff}: 0.63 mm, t_{on}: 10 ms; (b) P: 1.6 kW, r_{eff}: 0.63 mm, t_{on}: 14 ms; (c) P: 1.4 kW, r_{eff}: 0.50 mm, t_{on}: 0.15 s; (d) P: 1.4 kW, r_{eff}: 0.50 mm, t_{on}: 0.65 s.

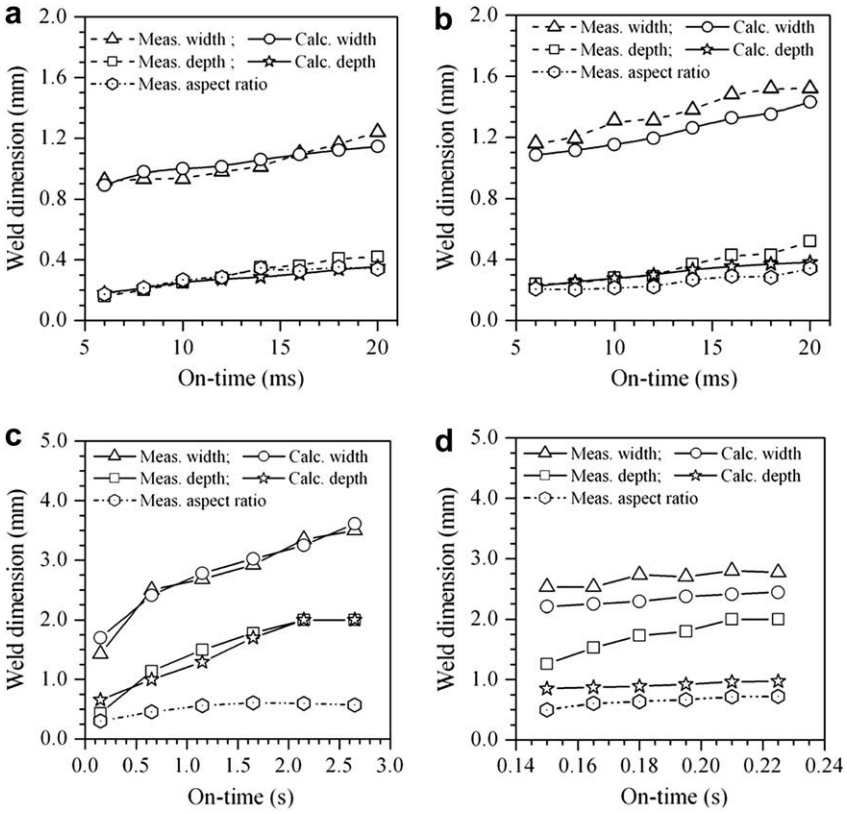

Fig. 5. Comparison of computed weld dimensions with corresponding measured results for various power densities. (a) 0.8 kW/mm^2, (b) 1.3 kW/mm^2, (c) 1.8 kW/mm^2 and (d) 2.8 kW/mm^2.

computed values of weld pool are always smaller against the corresponding measured results for laser power of 2.23 kW [Fig. 5(d)]. The maximum weld pool aspect ratio corresponding to laser powers of 1.0 kW and 1.6 kW is 0.34 [Fig. 5(a) and (b)] while the same varies from 0.25 at lower on-time to approximately 0.50 at the highest on-time at the laser power of 1.4 kW [Fig. 5(c)]. The values of weld pool aspect ratio corresponding to the laser power of 2.23 kW are well above 0.50 even at the smallest on-time [Fig. 5(d)]. It is also noteworthy that the power density corresponding to all the spot welds in Fig. 5(d) confirm to 2.8 kW/mm^2 that is sufficient to produce a stable keyhole within the low-carbon steel substrate [2]. It is thus imperative that the conduction heat transfer based numerical model will have limitations to reliably predict weld pool shapes in the case the mode of welding tends to be keyhole in nature either due to high power density or due to large on-time. Although the incorporation of an adaptive volumetric heat source within the growing melt portion of the substrate thickness could help to simulate relatively high power conduction mode laser spot welding, it is aptly clear from Fig. 5(d) that the same could not simulate the high penetration welding that is normal in keyhole mode.

The second major reason for the discrepancy in the computed and experimental weld dimension can be attributed to the choice of a single value of absorption coefficient for all the powers ranging from 1.0 kW to 2.23 kW. However, the advantage of the present model is that it reduces number of fitting parameters needed to represent the heat source and subsequent numerical calculations.

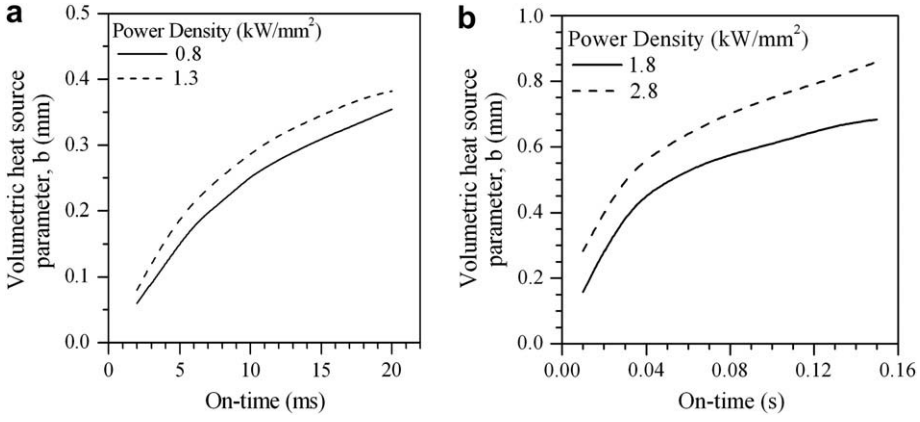

Fig. 6. Computed growth of the volumetric heat source parameter, *b*, with time.

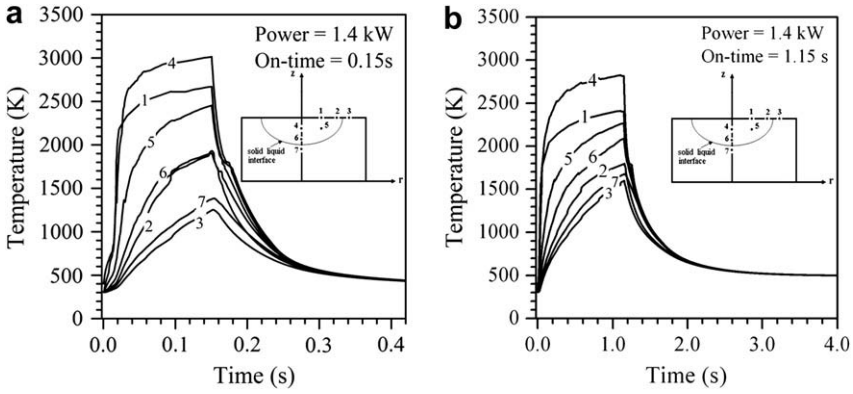

Fig. 7. Weld thermal cycle at monitoring locations 1–7 for 1.4 kW laser power and at on- times of (a) 0.15 s and (b) 1.15 s.

For example, De et al. [15,16] suggested the value of volumetric heat source parameter b (Fig. 4 and eq. (5)) to be equal to the complete sheet thickness at higher power, whereas at low power densities the value of b was determined by trial-and-error. However, the values of volumetric heat source parameters, in the present model, are determined adaptively following equation (5). To clarify further, the change in the computed values of the parameter b with progress in on-time is shown in Fig. 6(a) and (b) for four different power densities (Table 2). A steady increase in the computed value of the parameter b with on-time in all cases of power densities clearly indicates the adaptive adjustment of the volumetric heat source with the transient change in weld pool. It is, however, observed that at higher power densities, the computed value of the parameter b is not able to compensate for the greater rate of energy absorption in weld pool (Figs. 6(b) and 5(d)) and subsequently deeper weld penetration. A comparison of Figs. 6(b) and 5(d) clearly indicates that although the value of b increases thereby increasing the size of the volumetric heat source, it has under-predicted the weld penetration significantly. It is believed that at higher power densities, as the mode of welding tends to be keyhole in nature, rate of energy absorption from the laser beam into the weld pool is enhanced significantly that would have also required a significant enhancement in the value of absorption coefficient. However, to keep the modeling calculations tractable over a large range of process parameters, a single value of absorption coefficient is used for the volumetric heat source in the present model.

In the initial period of laser irradiation, the laser energy is absorbed in the substrate to initiate melting and till such point the heat source penetration is not possible. As melting of the substrate occurs, the laser beam energy is reached into the weld pool volume resulting in rapid increase in further melting of substrate. The rapid increase in the computed value of b up to certain on-time is an indication of such rapid increase in weld pool volume. The penetration of heat source in substrate is then gradual as considerable amount of heat is also dissipated by conduction through the bulk solid material. A slow down in the increase in the value of b in the later part of on-time indicates this phenomenon. The instantaneous value of b in turn represents the weld pool penetration at any specific time instant and thus, the higher value of b at greater laser power density corresponding to any time instant is well justified.

The numerical model is used further to calculate the thermal cycles experienced at a number of representative points within the weld pool and the heat affected zone. Fig. 7(a) and (b) shows the computed weld thermal cycles at different locations in the weld pool corresponding to a laser power of 1.4 kW and at two different on-times of 0.15 s and 1.15 s. Since the monitoring locations are selected such that they lie in the middle and near to the periphery of weld pool, the coordinates of these locations vary with the change in the weld pool dimensions. Fig. 7(a) and (b) depicts that the locations that are well within the weld pool (points 1, 4 and 5) experience relatively higher peak temperature than the points that are near to the periphery of the weld pool (points 6 and 7). However, the cooling rates at all the locations within the weld pool are extremely high and almost unanimous irrespective of their positions. The rate of cooling reduces exponentially beyond 500 K at all the monitoring locations. Considering the uniformity of the nature of the cooling curves at several locations within the weld pool, average values of the cooling rate of the weld pool at various values of temperature can be estimated further.

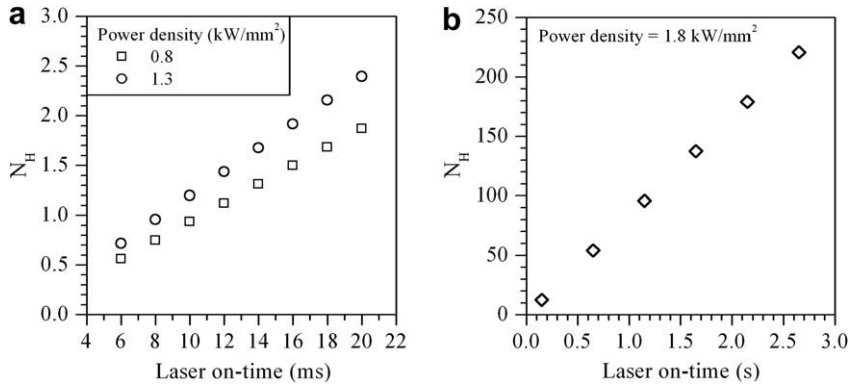

Fig. 8. Variation of non-dimensional heat index N_H on laser on-time.

To realize the combined influence of laser power density and thermophysical material properties on cooling rate, a non-dimensional heat index, N_H is expressed as

$$N_H = \frac{\left(\frac{P}{\pi r_{eff}^2}\right)(t_{on})\left(\frac{1}{D}\right)}{\rho C_p(T_L - T_0) + \rho L} \quad (22)$$

where P is the laser power (W), r_{eff} the spot radius (m), t_{on} the laser on-time (s), D the sheet thickness (m), ρ the density (kg m^{-3}), C_p the specific heat of the solid (J kg^{-1} K^{-1}), L the latent heat of fusion (J kg^{-1}), and T_L and T_0 are the liquidus and ambient temperatures (K), respectively. N_H can be considered as a ratio of total input energy per unit volume to the enthalpy needed to heat unit volume of the substrate material from ambient temperature to liquidus temperature. For a given sheet thickness and material properties, N_H increases with increase in either laser power density or on-time. For a fixed material and power density, N_H varies linearly with on-time. Fig. 8 depicts the nature of the variation of N_H with laser on-time and the quantitative estimation of N_H for three power density i.e. 0.8, 1.3 and 1.8 kW/mm^2 are described in Fig. 8. Fig. 8(a) shows that N_H ranges from 0.56 to 2.4 while the same varies from 12.5 to 221 in Fig. 8(b) since the power density as well as the on-time is high for the latter case.

The values of the average cooling rates in weld pool corresponding to two different values of temperature are plotted in Fig. 9 at different values of N_H. The values of N_H in Fig. 9 correspond to a laser power of 1.4 kW and various on-times. Fig. 9 shows that at lower values of N_H, the computed values of cooling rate at 1320 K are more than the same at 1055 K. As the value of N_H increases, the values of average cooling rates decrease considerably and become nearly same corresponding to both 1320 K and 1055 K. At higher values of N_H, the size of the weld pool increases considerably thereby reducing the value of the average cooling rate.

The present model thus makes it possible to effectively use a volumetric heat source in numerical simulation of conduction mode laser spot welding without the need of *a-priori* knowledge of the heat source parameters. This greatly eliminates the artifact associated with the representation of the laser beam in the form of a volumetric heat source. Subsequently, a reliable numerical model to analyze heat transfer in laser spot welding process using the conduction mode of heat transfer only has been achieved.

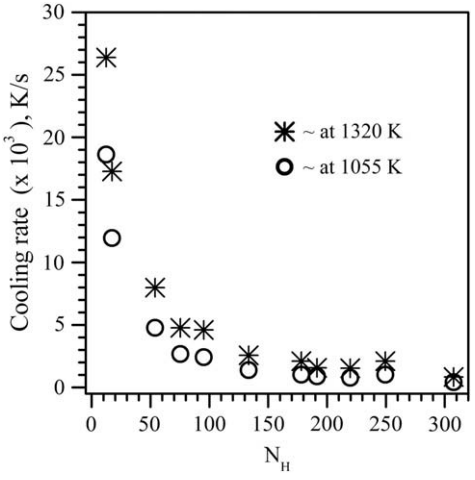

Fig. 9. Influence of non-dimensional parameter N_H on cooling rate.

5. Conclusions

A two-dimensional, axisymmetric, finite element model is developed to analyze heat transfer process in laser spot welding has been developed using a combination of surface heat flux and an adaptively defined volumetric heat source representation of the laser beam. The representation of laser beam as an adaptive volumetric heat source especially as the weld time increases describes a more realistic situation as the heat source penetrates into the substrate with time. The use of volumetric heat source was restricted earlier owing to the fact that the estimation of heat source parameters required the knowledge of the actual weld pool size as *a-priori*. The adaptive heat source suggested in the present study overcomes this restriction since the size of the volumetric source is decided based on the solid liquid boundary of the growing fusion zone. The calculated results of the weld pool at various values of laser power and on-times have agreed fairly well with the corresponding experimentally measured values for laser power of 1.0, 1.4 and 1.6 kW. The computed weld thermal cycle shows large cooling rates due to high peak temperature and short weld duration that are characteristics of laser spot welding. A unique non-dimensions parameter is used to embody the combined influence of the laser beam power density and the thermophysical properties of the sheet material on average cooling rate of the weld pool. The numerical model has experienced a major challenge in predicting weld pool shapes, in particular weld penetration, reliably at the highest power of 2.23 kW due to the possible presence of keyhole that could not be simulated. Overall, the use of an adaptive volumetric heat source improves the scope of the conduction heat transfer based numerical modeling of conduction mode laser welding process. Such model can be of significant help, in particular, when fast and repetitious *a-priori* calculations are in demand for understanding influences of process parameters on weld pool dimensions and subsequently designing a permissible range of process parameters for a desired sheet material and thickness.

Acknowledgements

The authors gratefully acknowledge the financial support being provided by the Department of Science & Technology, Government of INDIA (Grant no. SR/S3/MERC-043/2004) to carry out the present research work.

References

[1] X. He, T. DebRoy, P.W. Fuerscbach, Probing temperature during laser spot welding from vapor composition and modeling, J. Appl. Phys. 94 (10) (2003) 6949–6958.
[2] W.W. Duley, Laser Welding, John Wiley and Sons, New York, 1998.
[3] D. Rosenthal, Mathematical theory of heat distribution during and cutting, Weld. J. 20 (5) (1941) 220s–234s.
[4] N. Christensen, V.de L. Davies, K. Gjermundsen, Distribution of temperatures in arc welding, Br. Weld. J. 12 (1965) 54–75.
[5] T.D.S. Hook, A.E.F. Gick, Penetration welding with lasers, Weld. J. 52 (11) (1973) 492s–499s.
[6] G.J. Andrew, D.R. Atthey, Hydrodynamic limit to penetration of a material by a high-power beam, J. Phys. D: Appl. Phys. 9 (12) (1976) 2181–2194.
[7] A. Kaplan, A model of deep penetration laser welding based on calculation of the keyhole profile, J. Phys. D: Appl. Phys. 27 (9) (1994) 1805–1814.
[8] H.E. Cline, T.R. Anthony, Heat treating and melting material with a scanning laser or electron beam, J. Appl. J. Phys. D: Appl. Phys. 48 (9) (1977) 3895–3900.
[9] W. Guo, A. Kar, Determination of weld pool shape and temperature distribution by solving three dimensional phase change heat conduction, Sci. Technol. Weld. Joining 5 (5) (2000) 317–323.
[10] J. Mazumder, W.M. Steen, Heat transfer model for CW laser material processing, J. Phys. D: Appl. Phys. 51 (2) (1980) 941–947.
[11] T. Zacharia, S.A. David, J.M. Vitek, T. DebRoy, Heat transfer during Nd–YAG pulsed laser welding and its effect on solidification structure of austenitic stainless steels, Metall. Trans. A 20A (1989) 957–967.
[12] W. Pitscheneder, M. Grubock, K. Mundra, T. DebRoy, R. Ebner, Numerical and experimental investigation of conduction mode welding, in: Proc. of Third

International Seminar on Numerical Analysis of Weldability, Graz-Seggau, Austria, 1995, pp. 41–63.
[13] X. He, P.W. Fuerscbach, T. DebRoy, Heat transfer and fluid flow during laser spot welding of 304 stainless steel, J. Phys. D: Appl. Phys. 36 (2003) 1388–1398.
[14] J. Goldak, A. Chakravarti, M. Bibby, A new finite element model for welding heat sources, Metall. Trans. B 15 (1984) 299–305.
[15] A. De, S.K. Maiti, C.A. Walsh, H.K.D.H. Bhadeshia, Finite element simulation of laser spot welding, Sci. Technol. Weld. Joining 8 (5) (2003) 377–384.
[16] A. De, C.A. Walsh, S.K. Maiti, Prediction of cooling rate and microstructure in laser spot welds, Bhadeshia H.K.D.H. Sci. Technol. Weld. Joining 8 (6) (2003) 391–399.
[17] M.R. Frewin, D.A. Scott, Finite element model of pulsed laser welding, Weld. J. 78 (1999) 15s–21s.
[18] W.S. Chang, S.J. Na, A study on the prediction of the laser weld shape with varying heat source equations and the thermal distortion of a small structure in micro-joining, J. Mater. Process Technol. 120 (2002) 208–214.
[19] K. Hong, D.C. Weckman, A.B. Strong, W. Zheng, Modeling turbulent thermo-fluid flow in stationary gas tungsten arc weld pools, Sci. Technol. Weld. Joining 7 (3) (2002) 125–136.
[20] V.A. Vinokurov, Welding Stress and Distortion, Boston Spa, The British Library, England, 1977.
[21] O.C. Zienkiewicz, Finite Element Methods in Engineering, McGraw-Hill, London, 1977.
[22] C.A. Walsh, H.K.D.H. Bhadeshia, A. Lau, B. Matthias, R. Oesterlein, J. Drechsel, Characteristics of high-power diode–laser welds for industrial assembly, J. Laser Appl. 15 (2) (2003) 68–76.